

Molecular BioSystems

Accepted Manuscript



This is an *Accepted Manuscript*, which has been through the Royal Society of Chemistry peer review process and has been accepted for publication.

Accepted Manuscripts are published online shortly after acceptance, before technical editing, formatting and proof reading. Using this free service, authors can make their results available to the community, in citable form, before we publish the edited article. We will replace this *Accepted Manuscript* with the edited and formatted *Advance Article* as soon as it is available.

You can find more information about *Accepted Manuscripts* in the [Information for Authors](#).

Please note that technical editing may introduce minor changes to the text and/or graphics, which may alter content. The journal's standard [Terms & Conditions](#) and the [Ethical guidelines](#) still apply. In no event shall the Royal Society of Chemistry be held responsible for any errors or omissions in this *Accepted Manuscript* or any consequences arising from the use of any information it contains.



www.rsc.org/molecularbiosystems

**Exploring the prominent performance of CX-4945
derivatives as protein kinase CK2 inhibitors by a combined
computational study**

Xuwen Wang^a, Peichen Pan^a, Youyong Li^a, Dan Li^b, Tingjun Hou^{*a,b}

^aInstitute of Functional Nano & Soft Materials (FUNSOM) and Collaborative
Innovation Center of Suzhou Nano Science and Technology, Soochow University,
Suzhou, Jiangsu 215123, China.

^bCollege of Pharmaceutical Sciences, Zhejiang University, Hangzhou,
Zhejiang 310058, China

Corresponding author:

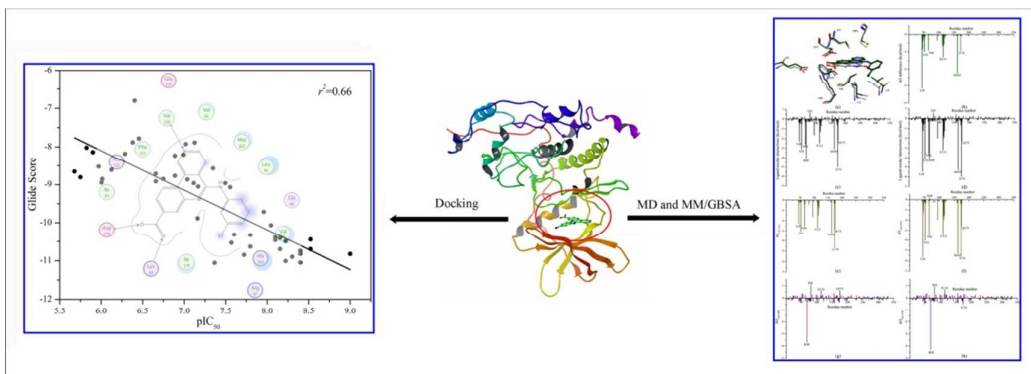
Tingjun Hou

E-mail: tingjunhou@hotmail.com or tingjunhou@zju.edu.cn

Phone: +86-512-65882039

Keywords: CK2 inhibitors, Molecular docking, Molecular dynamics (MD) simulations, MM/GBSA, MM/PBSA, Free energy calculation, Free energy decomposition

For Table of Contents Use Only



Abstract

Protein kinase CK2, also known as casein kinase II, is related to various cellular events and is a potential target for numerous cancers. In this study, we attempted to gain more insight into the inhibition process of CK2 by a series of CX-4945 derivatives through an integrated computational study that combines molecular docking, molecular dynamics (MD) simulations, and binding free energy calculations. Based on the binding poses predicted by molecular docking, the MD simulations were performed to explore the dynamic binding processes for ten selected inhibitors. Then, both Molecular Mechanics/Poisson Boltzmann Surface Area (MM/PBSA) and Molecular Mechanics/Generalized Born Surface Area (MM/GBSA) techniques were employed to predict the binding affinities of the studied systems. The predicted binding energies of the selected inhibitors correlate well with their experimental activities ($r^2=0.78$). The van der Waals term is the most favorable component for the total energies. The free energy decomposition on a per residue basis reveals that the residue K68 is essential for the electrostatic interactions between CK2 and the studied inhibitors and a numerous residues, including L45, V53, V66, F113, M163, and I174, play critical roles in forming van der Waals interactions with the inhibitors. Finally, a number of new derivatives were designed and the binding affinity and the predicted binding free energies of each designed molecule were obtained on the basis of molecular docking and MM/PBSA. It is expected that our research will benefit to the future rational design of novel and potent inhibitors of CK2.

Introduction

Protein kinase CK2 (formerly called casein kinase II) is a pleiotropic, ubiquitous, and highly conserved serine/threonine protein kinase for more than 300 protein substrates.¹⁻³ CK2 is comprised of two catalytic α subunits (α or α') and two regulatory β subunits that can form tetrameric complexes with various combinations of different subunits.⁴ The CK2 α subtype is widely expressed while the CK2 α' subtype is merely found in brain and testis.⁵ However, unlike most protein kinases, CK2 is constitutively active because its activation can be achieved without the phosphorylation by other protein kinases. Overexpression of CK2 was discovered in several human tumors⁶⁻¹³ and the key functions of CK2 in tumor initiation and progression make it an attractive therapeutic target.¹⁴⁻¹⁷ Thus, all these findings provide a rationale for the development of CK2 inhibitors as anti-cancer drugs. At present, both ATP-competitive inhibitors which have an overwhelming proportion and ATP-noncompetitive inhibitors of CK2 have been reported. The reported ATP-noncompetitive CK2 inhibitors provide opportunities for the development of allosteric inhibitors,^{18, 19} which target the CK2 β subunit or CK2 α -CK2 β interaction. As for the ATP-competitive inhibitors, several classes of them have been discovered,²⁰⁻³⁷ such as tetrabromo-1H-benzotriazole (TBB),³⁸ coumarin derivatives,³⁹ emodin,⁴⁰ (5-oxo-5,6-dihydroindolo[1,2-a]quinazolin-7-yl) acetic acid (IQA),⁴⁰ and pyrazolo[1,5-a][1,3,5]triazine derivatives,⁴¹ for representative examples. However, limited to selectivity, potency or possible potential long-term toxicity, none of the above compounds have reached clinical trials. Recently, the benzonaphthyridine derivative 31, CX-4945, was discovered and regarded as a rather promising, orally bioavailable ATP-competitive CK2 inhibitor, which was pushed into the clinical stage.⁴²⁻⁴⁶ Overall, there is still a dearth of potent and selective CK2 inhibitors nowadays. In our present work, a series of benzonaphthyridine derivatives including CX-4945 were studied through molecular modeling approaches. First of all, two different molecular docking protocols were utilized to determine the binding

geometries of the CX-4945 derivatives. Then, the dynamic binding processes of the selected inhibitors with diverse bioactivities were explicated by MD simulations. Furthermore, free energy calculations and decomposition were employed to highlight the crucial structural features for inhibitor binding. In addition, a series of novel derivatives of CX-4945 were designed according to the information we obtained.

Materials and Methods

1. Molecular Docking with Rigid Receptor. A total of 48 CX-4945 analogues with experimental inhibitory activities and defined stereochemistry were collected from the literature.⁴⁴ A majority of the studied molecules share similar scaffold and cover a wide range of IC_{50} from 1nM to 2.1 μ M, with four orders of magnitude. The 3-D structures of the studied molecules were sketched using the *Maestro* module in Schrödinger 9.0 and minimized with the *Macromodel* module in Schrödinger using the OPLS2005 force field.^{47,48} After that, all of these molecules were processed with the *Ligprep* module in Schrödinger to generate the correct tautomerization and protonated states.

The crystal structure of CK2 in complex with CX-4945 was retrieved from the RCSB Brookhaven Protein Data Bank (PDB entry: 3NGA),⁴⁹ which was served as the template structure for the following molecular docking calculations. The *Protein Preparation Wizard* in Schrödinger was used to add hydrogen atoms, remove the crystal waters, retain “A” chain of the homodimer with the inhibitor located in the active site, and minimize the structure with the OPLS2005 force field⁴⁸ until the root-mean-square deviation (RMSD) reached a maximum value of 0.3Å.

As for the grid generation, the binding box with a size of 10 Å × 10 Å × 10 Å was generated and centered on the co-crystallized ligand in the active site by using the default values in the *Receptor Grid Generation* module in Schrödinger. Then, the rigid receptor docking (*RRD*) protocol in *Glide* was employed to predict the binding geometries of the inhibitors with three precision scoring modes, including the high-throughput virtual screening (HTVS) mode, standard precision (SP) mode and

extra precision (XP) mode. In the docking process, the protein was fixed while the inhibitors were flexible. To soften the potential of the nonpolar parts of the inhibitors, the scaling factor of van der Waals radii of ligand atoms was set to 0.8 and the absolute value of partial atomic charge was set less than 0.15. Here, five poses per ligand were written out at most in the output files.

2. Induced Fit Docking. Apart from the *RRD* protocol, the induced fit docking (*IFD*) protocol in *Glide* was also used. In *IFD*, the flexibility of receptor is taken into account by combining a series of *Glide* and *Prime* processes. In the preliminary *Glide* docking step, the van der Waals radii scaling factor was 0.5 by default, and a maximum of 20 poses *per* ligand was retained. In the following *Prime* induced fit section, the residues within 5 Å away from the ligand were refined while the others were fixed, and the receptor-ligand complexes were minimized to an induced fit conformation. Finally, the best receptor-ligand complex was identified using a composite scoring function with the *Glide* XP scoring mode adopted for docking calculations.

3. Molecular Dynamics (MD) Simulations. The structures of ten inhibitors complexed with CK2 α given by *RRD* were submitted to the MD simulations. In order to select the ten inhibitors as logically as possible, the 48 inhibitors were divided into four categories according to the orders of the magnitude of their IC_{50} values. Subsequently, two or three inhibitors were selected symmetrically in each category. The structures and bioactivities of the ten selected inhibitors are shown in Table 1. The general AMBER force field (*gaff*)⁵⁰ and ff99SB force field⁵¹ were used to for ligand and protein, respectively. All the inhibitors were optimized by the semi-empirical AM1 method in Gaussian09 followed by the single-point (HF)/6-31G* calculation of electrostatic potentials⁵². Subsequently, the atomic partial charges of the inhibitors were obtained by the RESP fitting technique⁵³ in Amber11⁵⁴. The system was neutralized with the counter ions of Na⁺, and each system was immersed in a rectangular box of the TIP3P⁵⁵ water molecules, keeping 12 Å distance away from

any solute atom. Furthermore, the particle mesh Ewald (PME) algorithm was used to handle the long-range electrostatics⁵⁶ in molecular minimization and MD simulations. The *sander* program in AMBER11⁵⁴ was employed for the MM optimization and MD simulations.

Before MD simulations, each system was relaxed using a two-stage minimization strategy: the inhibitor and water molecules were first subjected to 1000 cycles of minimization (500 cycles of steepest descent and 500 cycles of conjugate gradient) with protein backbone constrained (50 kcal/mol/Å²), and then, the whole system was minimized by 1000 cycles of steepest descent and 4000 cycles of conjugate gradient minimization without any constrain. After minimization, each system was gradually heated in the NVT ensemble from 0 to 300 K over a period of 50 ps followed by a 5 ns NPT MD simulations with a target temperature of 300 K and a target pressure of 1 atm. The SHAKE procedure⁵⁷ was employed to constrain all bonds involving hydrogen atoms. The time step was set to 2 fs. The coordinates were saved every 10 ps during the MD sampling process.

4. MM/GBSA and MM/PBSA Binding Free Energy Calculation. For all the calculations below, a total of 100 snapshots from 2.0~5.0 ns were evenly extracted from the single MD trajectory at a time interval of 30 ps. Then, the absolute binding free energy (ΔG_{bind}) was predicted by applying the MM/GBSA and MM/PBSA approaches according to the following equation:⁵⁸⁻⁷⁵

$$\begin{aligned}\Delta G_{\text{bind}} &= G_{\text{complex}} - G_{\text{protein}} - G_{\text{ligand}} \\ &= \Delta H + \Delta G_{\text{solvation}} - T\Delta S \\ &= \Delta E_{\text{MM}} + \Delta G_{\text{GB/PB}} + \Delta G_{\text{SA}} - T\Delta S\end{aligned}\quad (1)$$

where G_{complex} , G_{protein} and G_{ligand} represent the free energies of complex, protein and ligand, respectively. ΔE_{MM} is the gas-phase interaction energy calculated using *sander*, including internal, electrostatic, and van der Waals energies, and the internal energy was cancelled based on the single MD trajectory. The solvation free energy $\Delta G_{\text{solvation}}$ was comprised of polar and nonpolar parts, which was denoted by $\Delta G_{\text{GB/PB}}$ and ΔG_{SA} ,

respectively. In the MM/GBSA calculations, the Onufriev's modified GB model (*igb=2*)⁷⁶ was used to calculate the polar desolvation free energy (ΔG_{GB}). In the MM/PBSA calculations, the polar desolvation free energy (ΔG_{PB}) was calculated by the PB solver implemented in the *pbsa* module in Amber11.⁵⁴ The radii optimized by Tan and Luo with respect to the reaction field energies computed in the TIP3P explicit solvents were used.⁷⁷ The grid size was defined as 0.5 Å. In the PB and GB calculations, the exterior dielectric constant (solvent) was set to 80 and the interior dielectric constant (solute) was set to 1, 2, or 4. The nonpolar contribution (ΔG_{SA}) was computed based on the solvent-accessible surface area (SASA) determined by the LCPO method: $\Delta G_{SA} = 0.0072 \times \Delta SASA$ ⁷⁸. In consideration of low prediction accuracy and expensive computational cost, the change of conformation entropy ($-T\Delta S$) was ignored here.^{79, 80}

5. MM/GBSA Binding Energy Decomposition Analysis. For the sake of illustrating the interactions between each protein residue and inhibitor, the MM/GBSA decomposition analysis supported by the *mm_pbsa* module in AMBER11 was performed.^{78, 81} The binding interaction of each residue-inhibitor pair consists of four components: van der Waals contribution (ΔG_{vdw}), electrostatic contribution (ΔG_{ele}) and polar contribution of desolvation (ΔG_{GB}) and the nonpolar contribution of desolvation (ΔG_{SA}), as shown in Equation 2:

$$\Delta G_{inhibitor-residue} = \Delta E_{vdw} + \Delta G_{ele} + \Delta G_{GB} + \Delta G_{SA} \quad (2)$$

The ΔG_{vdw} and ΔG_{ele} were calculated using the *sander* program in AMBER11. The GB model with the parameters developed by Onufriev et al. (*igb=2*)⁷⁶ was used to compute ΔG_{GB} . The ΔG_{SA} term was estimated based on the solvent-accessible surface area (SASA) with the ICOSA method.⁷⁸ The values of the exterior dielectric constant and the interior dielectric constant were set to 80 and 4, respectively, according to the previous results of the binding free energy calculation. Similarly, 100 snapshots extracted from 2.0 to 5.0 ns were used for the calculations of all energy components in Equation 2.

Results and Discussion

1. CK2/inhibitor complex models obtained by molecular docking. Although the 48 CX-4945 analogues (Table S1) share similar scaffold, their bioactivities are still quite different, which is exactly what we are interested in. The crystal structure of CK2 in complex with CX-4945 is available (PDB entry: 3NGA⁴⁹). For the rest of them, molecular docking technique was employed to predict their binding structures.

Above all, it is necessary to evaluate the reliability of the molecular docking methods. Therefore, the inhibitor CX-4945 obtained from the co-crystal structure was redocked into the binding site of CK2 using *IFD* with the XP scoring mode and *RRD* with three different scoring modes, including HTVS, SP, and XP. The conformation of CX-4945 with the lowest *Glide* docking score was adopted as the correct binding pose, which overlaps well with the co-crystallized structure of CX-4945. As shown in Figure S1 in the Supporting Materials, the root mean square deviation (RMSD) between the *Glide*-predicted pose and the co-crystallized structure of CX-4945 is approximately 0.03 Å for *RRD* with the HTVS scoring, 0.02 Å for *RRD* with the SP scoring, 0.02 Å for *RRD* with the XP scoring, and 0.72 Å for *IFD* with the XP scoring. Thus, both *RRD* and *IFD* show excellent performance for the prediction of the binding conformation of CX-4945.

Considering their remarkable performance for reproducing the crystal structure, *RRD* and *IFD* were both employed to predict the binding geometries of the 48 studied CX-4945 analogs. The linear correlation between the experimental pIC₅₀ and docking scores was also evaluated. As shown in Figure 1, the correlation coefficients (r^2) are 0.66, 0.63, 0.49 and 0.49 for *RRD* with HTVS, *RRD* with SP, *RRD* with XP and *IFD* with XP, respectively. The docking scores predicted by the two different docking protocols are summarized in Table S2 in the Supporting Materials. Although it has been reported that *IFD* performed better than *RRD* for some cases,^{68, 82} it is interesting to find that *RRD* with HTVS performed better than *RRD* with XP or *IFD* with XP in this study. This phenomenon demonstrates that the accuracy of different docking protocols is dependent with different systems. In a word, the approach of *RRD* with

HTVS is the optimal choice for our system, and the superposition of the binding poses of the 48 inhibitors (Figure S2) indicates that all these inhibitors share a similar binding mode in the active pocket of CK2. The docked structures afford valuable information for exploring structure-activity relationships of the studied inhibitors. For example, the binding modes of the inhibitors 1 and 36 predicted by *RRD* with HTVS are shown in Figure 2. For both of the inhibitors 1 and 36, the oxygen of the hydroxyl group can form two H-bonds with the ammonium group of Lys 68 and Asp 175. Furthermore, the inhibitor 36 can also form another H-bond with Val 116, which is favor of the binding affinity and is in agreement with the previous study.⁸³

2. MD simulations. What we obtained through molecular docking are merely the static binding configurations. In order to explore the dynamic binding features and clarify the dynamic interaction patterns between the inhibitors and CK2, the MD simulations for ten representative inhibitors/CK2 complexes, whose binding structures were predicted by *RRD* with HTVS, were implemented. The RMSD values of the C_{α} atoms of the inhibitor 1/CK2 and inhibitor 36/CK2 complexes during the production phase relative to the starting structures were calculated and displayed in Figure 3. It can be observed that the conformations of the these two complexes do not reach equilibrium until about 1500 ps, and the averaged C_{α} RMSDs are 1.56 ± 0.12 Å and 1.36 ± 0.10 Å, respectively, indicating that the fluctuation of the inhibitor 36/CK2 complex is less significant than that of the inhibitor 1/CK2 complex (the averaged RMSD and standard deviation of RMSD were calculated based on the snapshots from 1.5 to 5 ns). The RMSD values for the C_{α} atoms of the remaining eight protein/inhibitor complexes are shown in Figure S3.

Furthermore, as an example, the detailed analysis of root-square fluctuation (RMSF) *versus* residue number for the inhibitor 1/CK2 is illustrated in Figure 4. It is clear that relatively smaller dynamic fluctuations locate in the active site residues, such as the regions around the residues L45, V53, V66, K68, I95, N118, H160, M163, and W176. We can also observe that the regions around the residues S2, G185 and D271 exhibit much larger dynamic fluctuations since they locate in the non-active site

regions or around the N- and C- terminals.

3. MM/GBSA and MM/PBSA calculations. Considering the system-dependent property of MM/GBSA and MM/PBSA,⁶¹ both methods were employed to calculate the absolute binding free energies on the basis of three different solute dielectric constants (1, 2 and 4) for the ten selected inhibitors. The accuracy of the calculated results was evaluated by comparing the correlation coefficients between the experimental pIC₅₀ and the calculated binding free energies. It is encouraging to find that the results calculated with different methods and parameters are rather well consistent with the experimental affinities of the inhibitors (Figure 5). The highest correlation coefficient ($r^2=0.78$) was obtained with MM/PBSA when the solute dielectric constant was set to 4. Moreover, the method of MM/GBSA with the constant of 2 or 4 yields the same correlation coefficients ($r^2=0.72$), which are slightly lower than that of MM/PBSA, indicating that the latter is more suitable for our system. Based on the best result above, the energy components of the binding free energies for the ten selected inhibitors are summarized in Table 2. By comparing each term, we found that favorable van der Waals and electrostatic terms contribute greatly to ligand binding, meanwhile the non-polar solvation contributes a little. Furthermore, the correlations between each energy term and the predicted binding free energies were calculated and compared. It is found that the van der Waals term has the best correlation ($r^2=0.70$) while the others (the electrostatic term $r^2=0.36$, the non-polar solvation term $r^2=0.11$ and the polar solvation term $r^2=0.47$) have relatively worse correlations. Therefore, it can be concluded that the non-polar contribution, especially the van der Waals term, plays the dominant role in the binding of inhibitors. The reason should be attributed to the hydrophobic environment around the inhibitors, formed by the non-polar amino acid residues, such as L45, V53, V66, F113, M163, and I174.

4. MM/GBSA Binding Energy Decomposition Analysis. As we all know, the quantitative information of the energy contribution for each residue is extremely

beneficial to understand the binding mechanism. Therefore, in order to gain a deep understanding of the binding mode of interactions between the substituents of the inhibitors and the surrounding residues, the total binding free energy was decomposed on the basis of per residue. Here, the interaction spectrums for five representative inhibitors were systematically summarized and compared (Figures 6, 7 and 8).

The difference of the IC_{50} values between inhibitors 1 and 36 is the largest, and the structures of the two inhibitors are shown in Table 1. According to the results of the binding free energy calculations (Table 2), the predicted binding free energy for inhibitor 36 (-68.09 kcal/mol) is much lower than that of inhibitor 1 (-45.16 kcal/mol), which is consistent with the experimental data. Further analysis of the energy contribution shows that both of the van der Waals interaction and the electrostatic interaction between inhibitor 36 and CK2 (-44.30 kcal/mol and -25.37 kcal/mol) are much stronger than those between inhibitor 1 and CK2 (-29.50 kcal/mol and -16.09 kcal/mol). By systematically analyzing the difference between the inhibitor-residue interaction spectra of the inhibitors 1 and 36 complexes, we find that the favorable residues between the two systems are quite similar, including the residues L45, V53, V66, K68, F113, M163, I174 and D175 (Figures 6c and 6d). Interestingly, most of these residues are hydrophobic, and they form strong van der Waals interactions with inhibitors 1 and 36. However, there are six residues (L45, V53, V66, M163, H115 and I174) with the absolute value of difference equivalent to about or larger than 1 kcal/mol (Figure 6b), and all of them have stronger non-polar contributions (mainly the van der Waals interaction) with 36 than with 1. Especially, L45 and M163 show the largest difference (Figures 6e and 6f). Moreover, the comparison of the polar contributions shows that the polar interactions of K68 is the major contributor for both of the inhibitors 1 and 36 systems (Figures 6g and 6h), and the residue K68 can form H-bonds with both inhibitor 1 and inhibitor 36, at the same time, inhibitor 36 can also form one H-bond with Val 116. The major unfavorable interactions of the polar interactions are contributed from the residues E81, E114, and D175 in the inhibitor 1 system. However, in the inhibitor 36 complex, the unfavorable contribution of D175 is reduced.

For inhibitors 36 and 43 (Table 1), the obvious difference is at the substituent R1, where the CO₂H in inhibitor 36 was replaced by a C-(1*H*-tetrazol-5-yl) group in inhibitor 43. This replacement leads to a more than 10 kcal/mol change in the predicted binding free energy (Table 2). Meanwhile, the averaged binding poses of the two inhibitors are also significantly different (Figure 7a). The van der Waals interaction between inhibitor 36 and CK2 (-44.30 kcal/mol) is almost the same as quite similar to that between inhibitor 43 and CK2 (-42.57 kcal/mol), but the electrostatic interaction between inhibitor 36 and CK2 (-25.37 kcal/mol) is about twice lower than that between inhibitor 43 and CK2 (-13.09 kcal/mol), which may result from the structural difference at R2. Interestingly, the polar interaction ($\Delta E_{\text{ele}} + \Delta G_{\text{PB}}$) between inhibitor 36 and CK2 is effectively reduced due to its obvious unfavorable contribution of the polar desolvation term (6.99 kcal/mol). The favorable residues for both inhibitors are similar as well (Figures 7c and 7d), and they are the residues L45, V53, V66, K68, F113, M163, I174 and D175. There are seven residues with the absolute value of the energy difference more than 0.5 kcal/mol according to the comparison of the inhibitor-residue interaction spectrums of 36 and 43 (Figure 7b), among which the residues V66, K68, F113, H115 and I174 are more favorable to 36 than 43 and the other two residues N118 and H160 are more favorable to 43 than 36. The residue F113 shows the largest difference. The comparison of the non-polar interaction between each residue and 36 and that between each residue and 43 (Figures 7f and 7e) show that N118 is more favorable to 43 than 36, and it forms stronger interaction with the group 3-Cl phenyl of inhibitor (Figure 7a). Moreover, the comparison of the polar interaction between each residue and 36 and that of 43 shows that K68 contributes most to the difference of them and the residue D175 is one of the major unfavorable residue for the binding of inhibitor 43 to CK2 as well as the residues E81 and E114 for both 36/CK2 and 43/CK2 (Figures 7h and 7g). The spatial distribution of the related residues is shown in Figure 7a.

For inhibitors 9 and 23, the structural difference is in ring A and ring B (Table 1), and the IC₅₀ of inhibitor 23 is much smaller than that of inhibitor 9. Based on the predicted values, the binding affinity of inhibitor 23 (-57.44 kcal/mol) is lower than

that of inhibitor 9 (-48.85 kcal/mol). The energy component analysis shows that both the van der Waals interaction (-38.70 kcal/mol) and the electrostatic interaction (-18.86 kcal/mol) between inhibitor 23 and CK2 are stronger than those (-34.92 kcal/mol and -12.13 kcal/mol) between inhibitor 9 and CK2. There are six residues with differences larger than 1 kcal/mol (Figure 8b), among which three residues (L45, V66, and F113) produce stronger non-polar interactions (Figures 8e and 8f) and H115 produces stronger polar interaction with inhibitor 23 than with 9 while N118 and H160 contribute more polar interactions with inhibitor 9 than with inhibitor 23 (Figures 8g and 8h). For both inhibitors, K68 is the major polar interaction contributor. The spatial distribution of the related residues is illustrated in Figure 8a.

By comparing the results of molecular docking and energy decomposition analysis, we found that the protein-ligand interaction patterns predicted by these two approaches are consistent. For example, as shown in Figure 2, both inhibitors 1 and 36 can form an H-bond with the ammonium group of Lys68, and consistently, the energy decomposition analysis reveals that the residue Lys68 is the major contributor for the polar interactions (Figure 6). Moreover, by molecular docking, we know that both inhibitors 1 and 36 are surrounded by the non-polar residues, including L45, V53, V66, F113, M163, and I174, and the energy decomposition analysis shows that these residues form strong non-polar interaction with the inhibitors.

5. Insights into the design of potent inhibitors. Based on the results and discussions above, we find some information about the crucial interaction patterns between these inhibitors and CK2. First, the favorable residues (L45, V53, V66, K68, F113, M163, I174 and D175) for these inhibitors are quite similar. Interestingly, most of these residues are hydrophobic, and they create hydrophobic pockets for inhibitors to form strong van der Waals interactions. Second, the H-bonding interaction between the substituent at R1 and K68 is critical to achieve strong inhibitor binding. It is rational to take all these information into account when designing more potent inhibitors.

Finally, a series of derivatives were designed according to the above analysis, and the binding pose and affinity of each molecule was predicted by *RDD* with the HTVS

mode that has been proved to be more suitable for our system. Subsequently, in order to predict the binding free energies of these compounds, the MD simulations with 5ns were performed and the method of MM/PBSA was employed when the solute dielectric constant was set to 4. The results obtained above were shown in Table 3 as well as that of the control inhibitor 36 for its prominent bioactivity ($IC_{50} = 1$ nM). Compared with the inhibitor 36, these five compounds have rather well performance in not only docking scores but also the predicted binding free energies, indicating they are promising compounds. With the purpose of enhancing the van der Waals interactions with the residues N117, L45, M163 and other residues surrounding ring B, the hydrogen atom in the ring was replaced by isopropyl and 3-methyl-phenyl for compounds N1 and N2, respectively. Similarly, in order to enhance the favorable van der Waals interactions between 3-Cl-phenyl group and surrounding residues (such as L45 and V53), the nitrogen atom was substituted by a carbon atom for compound N3, which has improved docking score. Considering the potential toxicity of the halogen element in the 3-Cl-phenyl group, the chlorine atom was replaced by an ethyl group, which can form hydrophobic interaction for compound N4, and this substitution significantly improves the binding affinity of the inhibitor. Finally, the replacement of the hydrogen atom by a methyl near the carboxyl group can also improve the binding affinity for compound N5. Overall, these five designed compounds may be potential CK2 inhibitors with improved potency, and they deserve experimental verification in the future research.

Conclusions

In the present study, the interactions between CK2 and a series of CX-4945 derivatives were explored by using an integrated computational protocol, consisting of molecular docking, MD simulations, and binding free energy calculations. We found that the *Glide* docking with the HTVS scoring achieves the most optimal accuracy of prediction for our systems. Based on the MD simulations, the binding free energies were predicted by using the MM/PBSA and MM/GBSA approaches, and

MM/PBSA shows slightly better performance than MM/GBSA. According to the calculated results of MM/PBSA, the overall rank of the predicted binding free energies of the studied inhibitors is in excellent agreement with the experimental activities. Further decomposition of the overall binding free energies into individual energy terms indicates that the van der Waals energies are the dominant force for inhibitor binding. The decomposition of the binding free energy on a per-residue shows that the non-polar residues L45, V53, V66, F113, M163, I174 play critical roles in forming van der Waals interactions with the inhibitors. Moreover, the H-bonds between the carboxyl group of the inhibitors and the residue K68 are the major contributors for the electrostatic interactions and are also crucial for inhibitor binding. Finally, a number of derivatives were designed, among which five candidates showed great potency according to the calculations. Our study is beneficial for the further rational design of novel potent inhibitors of CK2.

Acknowledgments

This study was supported by the National Science Foundation of China (21173156), the National Basic Research Program of China (973 program, 2012CB932600), the Specialized Research Fund for the Doctoral Program of Higher Education (20123201110017), and the Priority Academic Program Development of Jiangsu Higher Education Institutions (PAPD).

References

1. L. A. Pinna, The raison D'Étre of constitutively active protein kinases: The lesson of CK2, *Accounts Chem. Res.*, 2003, **36**, 378-384.
2. F. Meggio and L. A. Pinna, One-thousand-and-one substrates of protein kinase CK2?, *Faseb J.*, 2003, **17**, 349-368.
3. J. S. Duncan and D. W. Litchfield, Too much of a good thing: The role of protein kinase CK2 in tumorigenesis and prospects for therapeutic inhibition of CK2, *BBA-Proteins Proteomics*, 2008, **1784**, 33-47.
4. D. W. Litchfield, Protein kinase CK2: structure, regulation and role in cellular decisions of life and death, *Biochem. J.*, 2003, **369**, 1-15.
5. B. Guerra, S. Siemer, B. Boldyreff and O. G. Issinger, Protein kinase CK2: evidence for a protein

- kinase CK2 beta subunit fraction, devoid of the catalytic CK2 alpha subunit, in mouse brain and testicles, *FEBS Lett.*, 1999, **462**, 353-357.
6. B. Guerra and O. G. Issinger, Protein kinase CK2 in human diseases, *Curr. Med. Chem.*, 2008, **15**, 1870-1886.
 7. G. M. Unger, A. T. Davis, J. W. Slaton and K. Ahmed, Protein kinase CK2 as regulator of cell survival: Implications for cancer therapy, *Curr. Cancer Drug Targets*, 2004, **4**, 77-84.
 8. R. A. Faust, S. Tawfic, A. T. Davis, L. A. Bubash and K. Ahmed, Antisense oligonucleotides against protein kinase CK2-alpha inhibit growth of squamous cell carcinoma of the head and neck in vitro, *Head Neck-J. Sci. Spec. Head Neck*, 2000, **22**, 341-346.
 9. E. Landesman-Bollag, R. Romieu-Mourez, D. H. Song, G. E. Sonenshein, R. D. Cardiff and D. C. Seldin, Protein kinase CK2 in mammary gland tumorigenesis, *Oncogene*, 2001, **20**, 3247-3257.
 10. K. Pistorius, G. Seitz, K. Remberger and O. G. Issinger, differential CKII activities in human colorectal mucosa, adenomas and carcinomas, *Onkologie*, 1991, **14**, 256-260.
 11. G. Stalter, S. Siemer, E. Becht, M. Ziegler, K. Remberger and O. G. Issinger, asymmetric expression of protein-kinase CK2 subunits in human kidney tumors, *Biochem. Biophys. Res. Commun.*, 1994, **202**, 141-147.
 12. P. O-charoenrat, V. Rusch, S. G. Talbot, I. Sarkaria, A. Viale, N. Socci, I. Ngai, P. Rao and B. Singh, Casein kinase II alpha subunit and C1-inhibitor are independent predictors of outcome in patients with squamous cell carcinoma of the lung, *Clin. Cancer Res.*, 2004, **10**, 5792-5803.
 13. S. Yenice, A. T. Davis, S. A. Goueli, A. Akdas, C. Limas and K. Ahmed, NUCLEAR CASEIN KINASE-2 (CK-2) ACTIVITY IN HUMAN NORMAL, BENIGN HYPERPLASTIC, AND CANCEROUS PROSTATE, *Prostate*, 1994, **24**, 11-16.
 14. S. Sarno and L. A. Pinna, Protein kinase CK2 as a druggable target, *Mol. Biosyst.*, 2008, **4**, 889-894.
 15. J. S. Kim, J. I. Eom, J. W. Cheong, A. J. Choi, J. K. Lee, W. I. Yang and Y. H. Min, Protein kinase CK2 alpha as an unfavorable prognostic marker and novel therapeutic target in acute myeloid leukemia, *Clin. Cancer Res.*, 2007, **13**, 1019-1028.
 16. M. Ruzzene and L. A. Pinna, Addiction to protein kinase CK2: A common denominator of diverse cancer cells?, *BBA-Proteins Proteomics*, 2010, **1804**, 499-504.
 17. M. J. Ku, J. W. Park, B. J. Ryu, Y.-J. Son, S. H. Kim and S. Y. Lee, CK2 inhibitor CX4945 induces sequential inactivation of proteins in the signaling pathways related with cell migration and suppresses metastasis of A549 human lung cancer cells, *Bioorg. Med. Chem. Lett.*, 2013, **23**, 5609-5613.
 18. R. Prudent and C. Cochet, New Protein Kinase CK2 Inhibitors: Jumping out of the Catalytic Box, *Chem. Biol.*, 2009, **16**, 112-120.
 19. R. Prudent, C. F. Sautel and C. Cochet, Structure-based discovery of small molecules targeting different surfaces of protein-kinase CK2, *BBA-Proteins Proteomics*, 2010, **1804**, 493-498.
 20. S. Sarno, S. Moro, F. Meggio, G. Zagotto, D. Dal Ben, P. Ghisellini, R. Battistutta, G. Zanotti and L. A. Pinna, Toward the rational design of protein kinase casein kinase-2 inhibitors, *Pharmacol. Ther.*, 2002, **93**, 159-168.
 21. S. Sarno, M. Ruzzene, P. Frascella, M. A. Pagano, F. Meggio, A. Zambon, M. Mazzorana, G. Di Maira, V. Lucchini and L. A. Pinna, Development and exploitation of CK2 inhibitors, *Mol. Cell. Biochem.*, 2005, **274**, 69-76.
 22. Y. Suzuki, J. Cluzeau, T. Hara, A. Hirasawa, G. Tsujimoto, S. Oishi, H. Ohno and N. Fujii,

- Structure-activity relationships of pyrazine-based CK2 inhibitors: Synthesis and evaluation of 2,6-disubstituted pyrazines and 4,6-disubstituted pyrimidines, *Arch. Pharm.*, 2008, **341**, 554-561.
23. R. Prudent, M. Lopez-Ramos, V. Moucadel, C. Barette, D. Grierson, L. Mouawad, J. C. Florent, L. Lafanechere, F. Schmidt and C. Cochet, Salicylaldehyde derivatives as new protein kinase CK2 inhibitors, *Biochim. Biophys. Acta-Gen. Subj.*, 2008, **1780**, 1412-1420.
 24. G. Cozza, A. Bortolato and S. Moro, How Druggable Is Protein Kinase CK2?, *Med. Res. Rev.*, 2010, **30**, 419-462.
 25. I. S. Sandholt, B. B. Olsen, B. Guerra and O. G. Issinger, Resorufin: a lead for a new protein kinase CK2 inhibitor, *Anti-Cancer Drugs*, 2009, **20**, 238-248.
 26. T. Nakaniwa, T. Kinoshita, Y. Sekiguchi, T. Tada, I. Nakanishi, K. Kitaura, Y. Suzuki, H. Ohno, A. Hirasawa and G. Tsujimoto, Structure of human protein kinase CK2 alpha 2 with a potent indazole-derivative inhibitor, *Acta Crystallogr. F-Struct. Biol. Cryst. Commun.*, 2009, **65**, 75-79.
 27. A. Najda-Bernatowicz, M. Lebska, A. Orzeszko, K. Kopanska, E. Krzywinska, G. Muszynska and M. Bretner, Synthesis of new analogs of benzotriazole, benzimidazole and phthalimide-potential inhibitors of human protein kinase CK2, *Bioorg. Med. Chem.*, 2009, **17**, 1573-1578.
 28. M. S. Hung, Z. D. Xu, Y. C. Lin, J. H. Mao, C. T. Yang, P. J. Chang, D. M. Jablons and L. You, Identification of hematein as a novel inhibitor of protein kinase CK2 from a natural product library, *BMC Cancer*, 2009, **9**.
 29. A. Gianoncelli, G. Cozza, A. Orzeszko, F. Meggio, Z. Kazimierczuk and L. A. Pinna, Tetraiodobenzimidazoles are potent inhibitors of protein kinase CK2, *Bioorg. Med. Chem.*, 2009, **17**, 7281-7289.
 30. G. Cozza, M. Mazzorana, E. Papinutto, J. Bain, M. Elliott, G. Di Maira, A. Gianoncelli, M. A. Pagano, S. Sarno, M. Ruzzene, R. Battistutta, F. Meggio, S. Moro, G. Zagotto and L. A. Pinna, Quinalizarin as a potent, selective and cell-permeable inhibitor of protein kinase CK2, *Biochem. J.*, 2009, **421**, 387-395.
 31. M. Lopez-Ramos, R. Prudent, V. Moucadel, C. F. Sautel, C. Barette, L. Lafanechere, L. Mouawad, D. Grierson, F. Schmidt, J. C. Florent, P. Filippakopoulos, A. N. Bullock, S. Knapp, J. B. Reiser and C. Cochet, New potent dual inhibitors of CK2 and Pim kinases: discovery and structural insights, *Faseb J.*, 2010, **24**, 3171-3185.
 32. Z. Hou, I. Nakanishi, T. Kinoshita, Y. Takei, M. Yasue, R. Misu, Y. Suzuki, S. Nakamura, T. Kure and H. Ohno, Structure-based design of novel potent protein kinase CK2 (CK2) inhibitors with phenyl-azole scaffolds, *J. Med. Chem.*, 2012, **55**, 2899-2903.
 33. M.-S. Hung, Z. Xu, Y. Chen, E. Smith, J.-H. Mao, D. Hsieh, Y.-C. Lin, C.-T. Yang, D. M. Jablons and L. You, Hematein, a casein kinase II inhibitor, inhibits lung cancer tumor growth in a murine xenograft model, *International journal of oncology*, 2013, **43**, 1517-1522.
 34. M. O. Chekanov, O. V. Ostrynska, A. R. Synyugin, V. G. Bdzhola and S. M. Yarmoluk, Design, synthesis and evaluation of 2-phenylisothiazolidin-3-one-1, 1-dioxides as a new class of human protein kinase CK2 inhibitors, *J. Enzyme Inhib. Med. Chem.*, 2013, 1-6.
 35. M. O. Chekanov, O. V. Ostrynska, S. S. Tarnavskyi, A. R. Synyugin, N. V. Briukhovetska, V. G. Bdzhola, A. E. Pashenko, A. A. Fokin and S. M. Yarmoluk, Design, synthesis and biological evaluation of 2-aminopyrimidinones and their 6-aza-analogs as a new class of CK2 inhibitors, *J. Enzyme Inhib. Med. Chem.*, 2013, 1-8.

36. A. G. Golub, V. G. Bdzhola, O. V. Ostrynska, I. V. Kyszenia, V. M. Sapelkin, A. O. Prykhod'ko, O. P. Kukhareno and S. M. Yarmoluk, Discovery and characterization of synthetic 4'-hydroxyflavones—New CK2 inhibitors from flavone family, *Bioorg. Med. Chem.*, 2013, **21**, 6681-6689.
37. X. Cheng, K.-H. Merz, S. Vatter, J. Christ, S. Wölfl and G. Eisenbrand, 7, 7'-Diazaindirubin-A small molecule inhibitor of casein kinase 2 in vitro and in cells, *Bioorg. Med. Chem.*, 2014, **22**, 247-255.
38. R. Szyszka, N. Grankowski, K. Felczak and D. Shugar, halogenated benzimidazoles and benzotriazoles as selective inhibitors of protein-kinases CK-i and CK-ii from *saccharomyces-cerevisiae* and other sources, *Biochem. Biophys. Res. Commun.*, 1995, **208**, 418-424.
39. J. W. Critchfield, J. E. Coligan, T. M. Folks and S. T. Butera, Casein kinase II is a selective target of HIV-1 transcriptional inhibitors, *Proceedings of the National Academy of Sciences of the United States of America*, 1997, **94**, 6110-6115.
40. H. Yim, Y. H. Lee, C. H. Lee and S. K. Lee, Emodin, an anthraquinone derivative isolated from the rhizomes of *Rheum palmatum*, selectively inhibits the activity of casein kinase II as a competitive inhibitor, *Planta Med.*, 1999, **65**, 9-13.
41. E. Vangrevelinghe, K. Zimmermann, J. Schoepfer, R. Portmann, D. Fabbro and P. Furet, Discovery of a potent and selective protein kinase CK2 inhibitor by high-throughput docking, *J. Med. Chem.*, 2003, **46**, 2656-2662.
42. Z. Nie, C. Perretta, P. Erickson, S. Margosiak, R. Almassy, J. Lu, A. Averill, K. M. Yager and S. S. Chu, Structure-based design, synthesis, and study of pyrazolo 1,5-a 1,3,5 triazine derivatives as potent inhibitors of protein kinase CK2, *Bioorg. Med. Chem. Lett.*, 2007, **17**, 4191-4195.
43. A. Siddiqui-Jain, D. Drygin, N. Streiner, P. Chua, F. Pierre, S. E. O'Brien, J. Bliesath, M. Omori, N. Huser, C. Ho, C. Proffitt, M. K. Schwaebe, D. M. Ryckman, W. G. Rice and K. Anderes, CX-4945, an Orally Bioavailable Selective Inhibitor of Protein Kinase CK2, Inhibits Prosurvival and Angiogenic Signaling and Exhibits Antitumor Efficacy, *Cancer Res.*, 2010, **70**, 10288-10298.
44. F. Pierre, P. C. Chua, S. E. O'Brien, A. Siddiqui-Jain, P. Bourbon, M. Haddach, J. Michaux, J. Nagasawa, M. K. Schwaebe, E. Stefan, A. Vialettes, J. P. Whitten, T. K. Chen, L. Darjania, R. Stansfield, K. Anderes, J. Bliesath, D. Drygin, C. Ho, M. Omori, C. Proffitt, N. Streiner, K. Trent, W. G. Rice and D. M. Ryckman, Discovery and SAR of 5-(3-Chlorophenylamino)benzo c 2,6 naphthyridine-8-carboxylic Acid (CX-4945), the First Clinical Stage Inhibitor of Protein Kinase CK2 for the Treatment of Cancer, *J. Med. Chem.*, 2011, **54**, 635-654.
45. R. Battistutta, G. Cozza, F. Pierre, E. Papinutto, G. Lolli, S. Sarno, S. E. O'Brien, A. Siddiqui-Jain, M. Haddach, K. Anderes, D. M. Ryckman, F. Meggio and L. A. Pinna, Unprecedented Selectivity and Structural Determinants of a New Class of Protein Kinase CK2 Inhibitors in Clinical Trials for the Treatment of Cancer, *Biochemistry*, 2011, **50**, 8478-8488.
46. L. Martins, P. Lúcio, A. Melão, I. Antunes, B. Cardoso, R. Stansfield, M. Bertilaccio, P. Ghia, D. Drygin and M. Silva, Activity of the clinical-stage CK2-specific inhibitor CX-4945 against chronic lymphocytic leukemia, *Leukemia*, 2013.
47. M. Schrödinger, NY, 2009.
48. G. A. Kaminski, R. A. Friesner, J. Tirado-Rives and W. L. Jorgensen, Evaluation and reparametrization of the OPLS-AA force field for proteins via comparison with accurate quantum chemical calculations on peptides, *Journal of Physical Chemistry B*, 2001, **105**,

- 6474-6487.
49. A. D. Ferguson, P. R. Sheth, A. D. Basso, S. Paliwal, K. Gray, T. O. Fischmann and H. V. Le, Structural basis of CX-4945 binding to human protein kinase CK2, *FEBS Lett.*, 2011, **585**, 104-110.
 50. J. M. Wang, R. M. Wolf, J. W. Caldwell, P. A. Kollman and D. A. Case, Development and testing of a general amber force field, *J. Comput. Chem.*, 2004, **25**, 1157-1174.
 51. V. Hornak, R. Abel, A. Okur, B. Strockbine, A. Roitberg and C. Simmerling, Comparison of multiple Amber force fields and development of improved protein backbone parameters, *Proteins: Struct., Funct., Bioinf.*, 2006, **65**, 712-725.
 52. M. Frisch, G. Trucks, H. Schlegel, G. Scuseria, M. Robb, J. Cheeseman, J. Montgomery Jr, T. Vreven, K. Kudin and J. Burant, Gaussian 03, revision D. 01, *Gaussian, Inc.: Wallingford, CT*, 2004.
 53. C. I. Bayly, P. Cieplak, W. D. Cornell and P. A. Kollman, A well-behaved electrostatic potential based method using charge restraints for deriving atomic charges: the RESP model, *J. Phys. Chem.*, 1993, **97**, 10269-10280.
 54. D. A. Case, T. E. Cheatham, T. Darden, H. Gohlke, R. Luo, K. M. Merz, A. Onufriev, C. Simmerling, B. Wang and R. J. Woods, The Amber biomolecular simulation programs, *J. Comput. Chem.*, 2005, **26**, 1668-1688.
 55. W. L. Jorgensen, J. Chandrasekhar, J. D. Madura, R. W. Impey and M. L. Klein, Comparison of simple potential functions for simulating liquid water, *J Chem Phys*, 1983, **79**, 926-935.
 56. T. Darden, D. York and L. Pedersen, PARTICLE MESH EWALD - AN N.LOG(N) METHOD FOR EWALD SUMS IN LARGE SYSTEMS, *J. Chem. Phys.*, 1993, **98**, 10089-10092.
 57. J. P. Ryckaert, G. Ciccotti and H. J. C. Berendsen, Numerical integration of the cartesian equations of motion of a system with constraints: molecular dynamics of n-alkanes, *J. Comput. Chem.*, 1977, **23**, 327-341.
 58. P. A. Kollman, I. Massova, C. Reyes, B. Kuhn, S. H. Huo, L. Chong, M. Lee, T. Lee, Y. Duan, W. Wang, O. Donini, P. Cieplak, J. Srinivasan, D. A. Case and T. E. Cheatham, Calculating structures and free energies of complex molecules: Combining molecular mechanics and continuum models, *Accounts Chem. Res.*, 2000, **33**, 889-897.
 59. J. M. Wang, T. J. Hou and X. J. Xu, Recent Advances in Free Energy Calculations with a Combination of Molecular Mechanics and Continuum Models, *Curr. Comput.-Aided Drug Des.*, 2006, **2**, 287-306.
 60. T. Hou, N. Li, Y. Li and W. Wang, Characterization of Domain-peptide Interaction Interface: Prediction of SH3 Domain-Mediated Protein-protein Interaction Network in Yeast by Generic Structure-Based Models, *J. Proteome Res.*, 2012, **11**, 2982.
 61. T. Hou, J. Wang, Y. Li and W. Wang, Assessing the performance of the MM/PBSA and MM/GBSA methods: I. The accuracy of binding free energy calculations based on molecular dynamics simulations, *J. Chem. Inf. Model.*, 2011, **51**, 69-82.
 62. T. J. Hou, Y. Y. Li and W. Wang, Prediction of peptides binding to the PKA RII alpha subunit using a hierarchical strategy, *Bioinformatics*, 2011, **27**, 1814-1821.
 63. T. J. Hou, J. Wang, Y. Y. Li and W. Wang, Assessing the performance of the molecular mechanics/Poisson Boltzmann surface area and molecular mechanics/generalized Born surface area methods. II. The accuracy of ranking poses generated from docking, *J. Comput. Chem.*, 2011, **32**, 866-877.

64. S. Huo, J. Wang, P. Cieplak, P. A. Kollman and I. D. Kuntz, Molecular dynamics and free energy analyses of cathepsin D-inhibitor interactions: insight into structure-based ligand design, *J. Med. Chem.*, 2002, **45**, 1412-1419.
65. L. Li, Y. Y. Li, L. L. Zhang and T. J. Hou, Theoretical Studies on the Susceptibility of Oseltamivir against Variants of 2009 A/H1N1 Influenza Neuraminidase, *J. Chem Inf. Model.*, 2012, **52**, 2715-2729.
66. H. Liu, X. Yao, C. Wang and J. Han, In silico identification of the potential drug resistance sites over 2009 influenza A (H1N1) virus neuraminidase, *Mol. Pharmaceut.*, 2010, **7**, 894-904.
67. W. W. Xue, D. B. Pan, Y. Yang, H. X. Liu and X. J. Yao, Molecular modeling study on the resistance mechanism of HCV NS3/4A serine protease mutants R155K, A156V and D168A to TMC435, *Antiviral Res.*, 2012, **93**, 126-137.
68. L. Xu, Y. Li, L. Li, S. Zhou and T. Hou, Understanding microscopic binding of macrophage migration inhibitory factor with phenolic hydrazones by molecular docking, molecular dynamics simulations and free energy calculations, *Mol. Biosyst.*, 2012, **8**, 2260-2273.
69. W. W. Xue, J. Qi, Y. Yang, X. J. Jin, H. X. Liu and X. J. Yao, Understanding the effect of drug-resistant mutations of HIV-1 intasome on raltegravir action through molecular modeling study, *Mol. Biosyst.*, 2012, **8**, 2135-2144.
70. Y. Yang, J. Qin, H. X. Liu and X. J. Yao, Molecular Dynamics Simulation, Free Energy Calculation and Structure-Based 3D-QSAR Studies of B-RAF Kinase Inhibitors, *J. Chem. Inf. Model.*, 2011, **51**, 680-692.
71. W. Xue, X. Jin, L. Ning, M. Wang, H. Liu and X. Yao, Exploring the Molecular Mechanism of Cross-Resistance to HIV-1 Integrase Strand Transfer Inhibitors by Molecular Dynamics Simulation and Residue Interaction Network Analysis, *J. Chem. Inf. Model.*, 2012, **53**, 210-222.
72. Y. Yang, H. Liu and X. Yao, Understanding the molecular basis of MK2-p38 α signaling complex assembly: insights into protein-protein interaction by molecular dynamics and free energy studies, *Mol. Biosystems*, 2012, **8**, 2106-2118.
73. Y. Yang, Y. Shen, S. Li, N. Jin, H. Liu and X. Yao, Molecular dynamics and free energy studies on Aurora kinase A and its mutant bound with MLN8054: insight into molecular mechanism of subtype selectivity, *Mol. Biosystems*, 2012, **8**, 3049-3060.
74. Y. Yang, Y. Shen, H. Liu and X. Yao, Molecular Dynamics Simulation and Free Energy Calculation Studies of the binding mechanism of allosteric inhibitors with p38 α MAP kinase, *J. Chem. Inf. Model.*, 2011, **51**, 3235-3246.
75. Q. Xue, J.-L. Zhang, Q.-C. Zheng, Y.-L. Cui, L. Chen, W.-T. Chu and H.-X. Zhang, Exploring the Molecular Basis of dsRNA Recognition by Mss116p Using Molecular Dynamics Simulations and Free-Energy Calculations, *Langmuir*, 2013, **29**, 11135-11144.
76. A. Onufriev, D. Bashford and D. A. Case, Exploring protein native states and large-scale conformational changes with a modified generalized born model, *Proteins*, 2004, **55**, 383-394.
77. C. Tan, L. Yang and R. Luo, How well does Poisson-Boltzmann implicit solvent agree with explicit solvent? A quantitative analysis, *J. Phys. Chem. B.*, 2006, **110**, 18680-18687.
78. H. Gohlke, C. Kiel and D. A. Case, Insights into protein-protein binding by binding free energy calculation and free energy decomposition for the Ras-Raf and Ras-RaIGDS complexes, *J. Mol. Biol.*, 2003, **330**, 891-913.
79. T. Hou, Y. Li and W. Wang, Prediction of peptides binding to the PKA RIIa subunit using a

- hierarchical strategy, *Bioinformatics*, 2011, **27**, 1814-1821.
80. T. Hou and R. Yu, Molecular dynamics and free energy studies on the wild-type and double mutant HIV-1 protease complexed with amprenavir and two amprenavir-related inhibitors: mechanism for binding and drug resistance, *J. Med. Chem.*, 2007, **50**, 1177-1188.
81. T. Hou and W. Zhang, Characterization of domain-peptide interaction interface: a case study on the amphiphysin-1 SH3 domain, *J. Mol. Biol.*, 2008, **376**, 1201-1214.
82. J. Du, H. J. Sun, L. L. Xi, J. Z. Li, Y. Yang, H. X. Liu and X. J. Yao, Molecular Modeling Study of Checkpoint Kinase 1 Inhibitors by Multiple Docking Strategies and Prime/MM-GBSA Calculation, *J. Comput. Chem.*, 2011, **32**, 2800-2809.
83. H. B. Liu, X. Wang, J. Wang, J. H. Wang, Y. Li, L. Yang and G. H. Li, Structural Determinants of CX-4945 Derivatives as Protein Kinase CK2 Inhibitors: A Computational Study, *Int. J. Mol. Sci.*, 2011, **12**, 7004-7021.

Legend of the Figures

Figure 1. The correlation between the experimental pIC_{50} and the docking scores predicted by (a) *RRD* with HTVS, (b) *RRD* with SP, (c) *RRD* with XP and (d) *IFD* with XP.

Figure 2. (a) The schema diagrams of the interactions (a) between inhibitor 1 and CK2 and (b) between inhibitor 36 and CK2.

Figure 3. Root-mean-square displacement (RMSD) of the backbone C_{α} atoms of the CK2/inhibitor complexes (1 and 36) with respect to the first snapshot as a function of time.

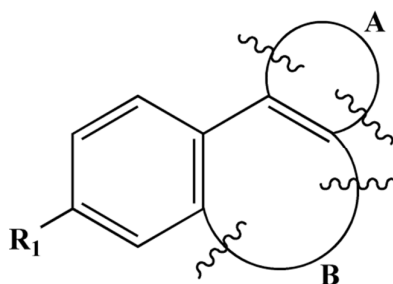
Figure 4. Root-mean-square fluctuation (RMSF) of backbone atoms *versus* residue number of the CK2/inhibitor 1 complex.

Figure 5. The correlations between the experimental bioactivities and (a) the docking scores predicted by *RRD* with HTVS, (b) the binding free energies predicted by MM/PBSA with solute dielectric constant of 4, (c) the binding free energies predicted by MM/GBSA with the solute dielectric constant of 2, and (d) the binding free energies predicted by MM/GBSA with the solute dielectric constant of 4 for ten selected inhibitors.

Figure 6. (a) The comparison of the averaged structures for the 1/CK2 and 36/CK2 complexes (carbon atoms are colored in gray and dark green, respectively); (b) energy difference of each residue to the binding of 1 and 36; the inhibitor-residue interaction spectra for the individual energy terms for (c) the 1/CK2 complex and (d) the 36/CK2 complex; the non-polar energy ($\Delta E_{\text{vdw}} + \Delta G_{\text{SA}}$) for (e) the 1/CK2 complex and (f) the 36/CK2 complex; the polar energy ($\Delta E_{\text{ele}} + \Delta G_{\text{GB}}$) for (g) the 1/CK2 complex and (h) the 36/CK2 complex.

Figure 7. (a) The comparison of the averaged structures for the 43/CK2 and 36/CK2 complexes (carbon atoms are colored in pink and dark green, respectively); (b) energy difference of each residue to the binding of 43 and 36; the inhibitor-residue interaction spectra for the individual energy terms for (c) the 43/CK2 complex and (d) the 36/CK2 complex; the non-polar energy ($\Delta E_{\text{vdw}} + \Delta G_{\text{SA}}$) for (e) the 43/CK2 complex and (f) the 36/CK2 complex; the polar energy ($\Delta E_{\text{ele}} + \Delta G_{\text{GB}}$) for (g) the 43/CK2 complex and (h) the 36/CK2 complex.

Figure 8. (a) The comparison of the averaged structures for the 9/CK2 and 23/CK2 complexes (carbon atoms are colored in plum and yellow green, respectively); (b) energy difference of each residue to the binding of 9 and 23; the inhibitor-residue interaction spectra for the individual energy terms for (c) the 9/CK2 complex and (d) the 23/CK2 complex; the non-polar energy ($\Delta E_{\text{vdw}} + \Delta G_{\text{SA}}$) for (e) the 9/CK2 complex and (f) the 23/CK2 complex; the polar energy ($\Delta E_{\text{ele}} + \Delta G_{\text{GB}}$) for (g) the 9/CK2 complex and (h) the 23/CK2 complex.

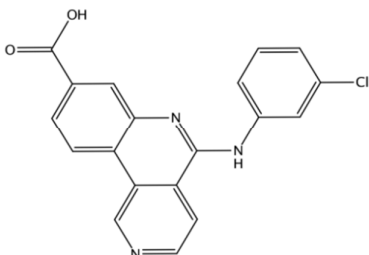
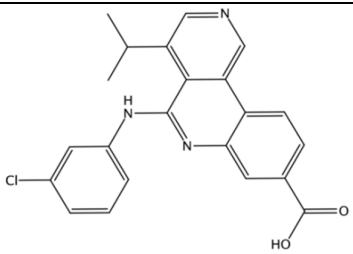
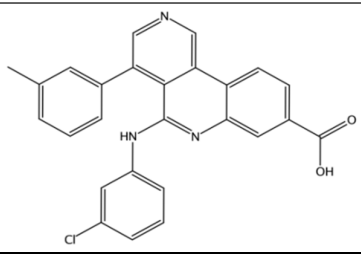
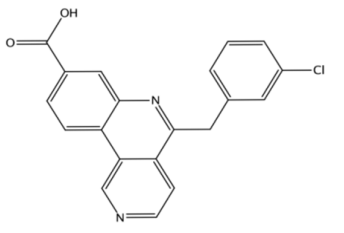
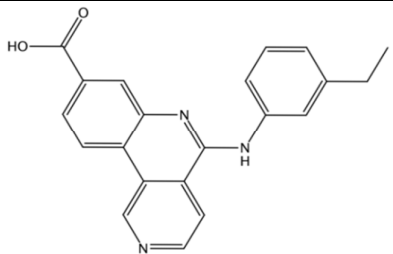
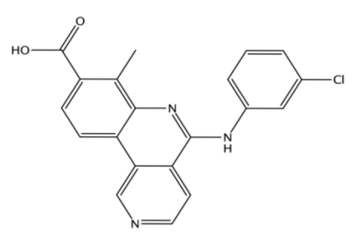
Table 1. Structures and biological activities of the ten selected inhibitors

NO.	A	B	R ₁	IC ₅₀ (nM)	pIC ₅₀
1	-S-CH=CH-	-CO-NH-	CO ₂ H	2100	5.68
2	-S-CH=CH-	-CO-N((CH ₂) ₃ OH)-	CO ₂ H	1500	5.82
6	-S-CH=CH-	-(C-NH(CH ₂) ₂ NMe ₂)=N-	CO ₂ H	102	6.99
9	-S-CH=CH-	-(C-NMe-phenyl)=N-	CO ₂ H	1070	5.97
12	-S-CH=CH-	-(C-NH(CH ₂) ₂ Ph)=N-	CO ₂ H	516	6.29
23	-CH=N-CH=CH-	-(C-NH-phenyl)=N-	CO ₂ H	6	8.22
28	-CH=N-CH=CH-	-(C-NH(CH ₂) ₂ O- <i>i</i> -Pr)=N-	CO ₂ H	11	7.96
36	-CH=N-CH=CH-	-(C-NH-(3-Cl-phenyl))=N-	CO ₂ H	1	9.00
38	-CH=N-CH=CH-	-(C-NH-(3-acetylenyl-phenyl))=N-	CO ₂ H	3	8.52
43	-CH=N-CH=CH-	-(C-NH-(3-Cl-phenyl))=N-	C-(1 <i>H</i> -tetrazol-5-yl)	45	7.35

Table 2. The predicted binding free energies and the individual energy components for the studied inhibitors (kcal/mol)

No.	E_{vdw}	E_{ele}	G_{SA}	G_{PB}	G_{pred}	pIC ₅₀
1	-29.50±2.47	-16.09±3.41	-4.23±0.11	4.65±0.64	-45.16±2.87	5.68
2	-33.74±3.16	-21.56±2.90	-5.01±0.22	5.86±0.58	-54.45±3.37	5.82
6	-40.28±2.88	-9.45±3.19	-5.76±0.30	3.92±0.73	-51.57±3.83	6.99
9	-34.92±3.10	-12.13±1.66	-5.41±0.21	3.61±0.33	-48.85±3.14	5.97
12	-40.08±2.52	-11.91±1.38	-5.73±0.17	3.81±0.30	-53.91±2.58	6.29
23	-38.70±2.78	-18.86±2.09	-4.93±0.33	5.06±0.43	-57.44±3.05	8.22
28	-42.08±2.79	-18.74±2.58	-5.71±0.18	5.56±0.56	-60.97±3.35	7.96
36	-44.30±2.63	-25.37±1.72	-5.41±0.12	6.99±0.37	-68.09±2.60	9.00
38	-46.62±2.83	-18.99±2.46	-5.62±0.19	5.36±0.55	-65.87±3.35	8.52
43	-42.57±2.98	-13.09±2.83	-5.58±0.26	4.39±0.54	-56.86±3.24	7.35

Table 3. Structures and Glide docking scores and the predicted binding free energies for inhibitor 36 and five designed compounds (kcal/mol)

Compounds	Structures	Docking Scores	G_{pred}
36		-10.77	-68.09
N1		-11.05	-66.02
N2		-10.91	-71.34
N3		-11.09	-56.43
N4		-10.77	-62.67
N5		-11.07	-64.76

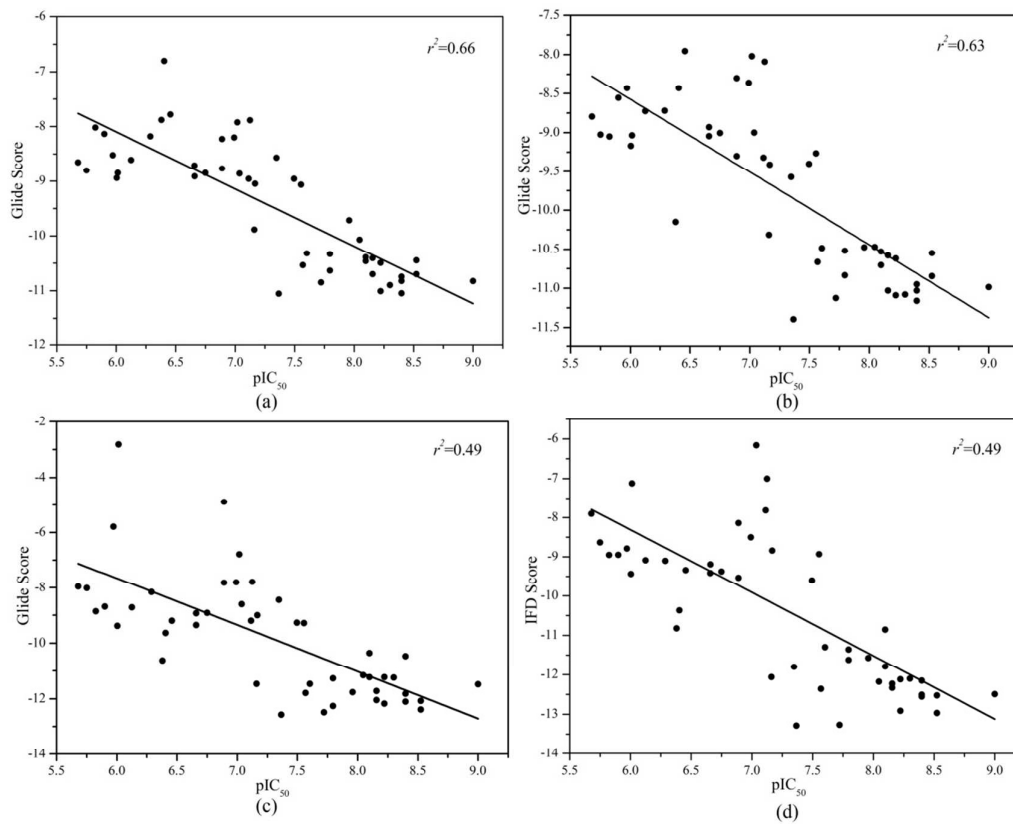


Figure 1

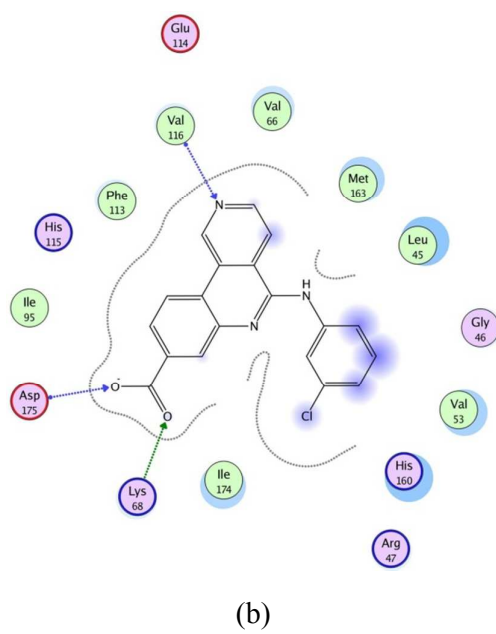
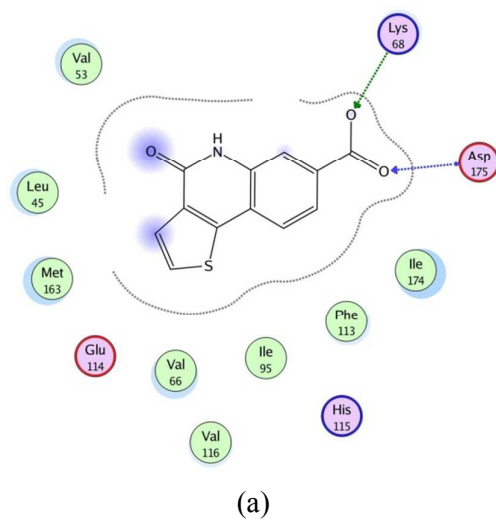


Figure 2

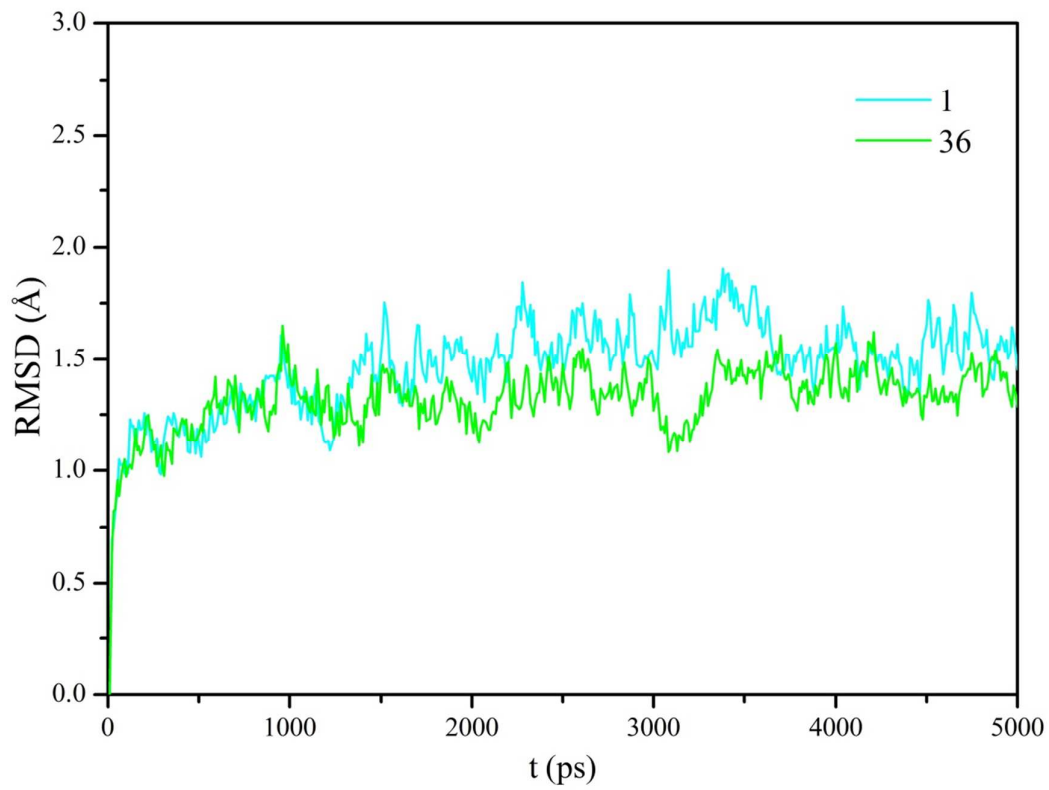


Figure 3

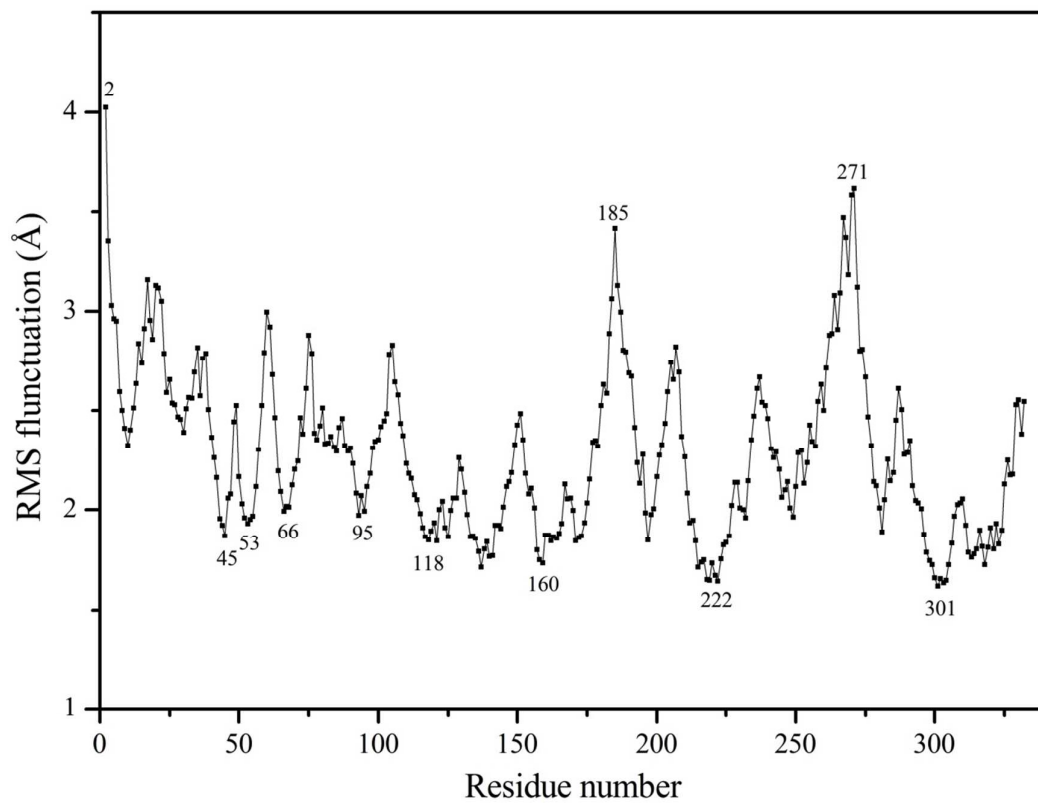


Figure 4

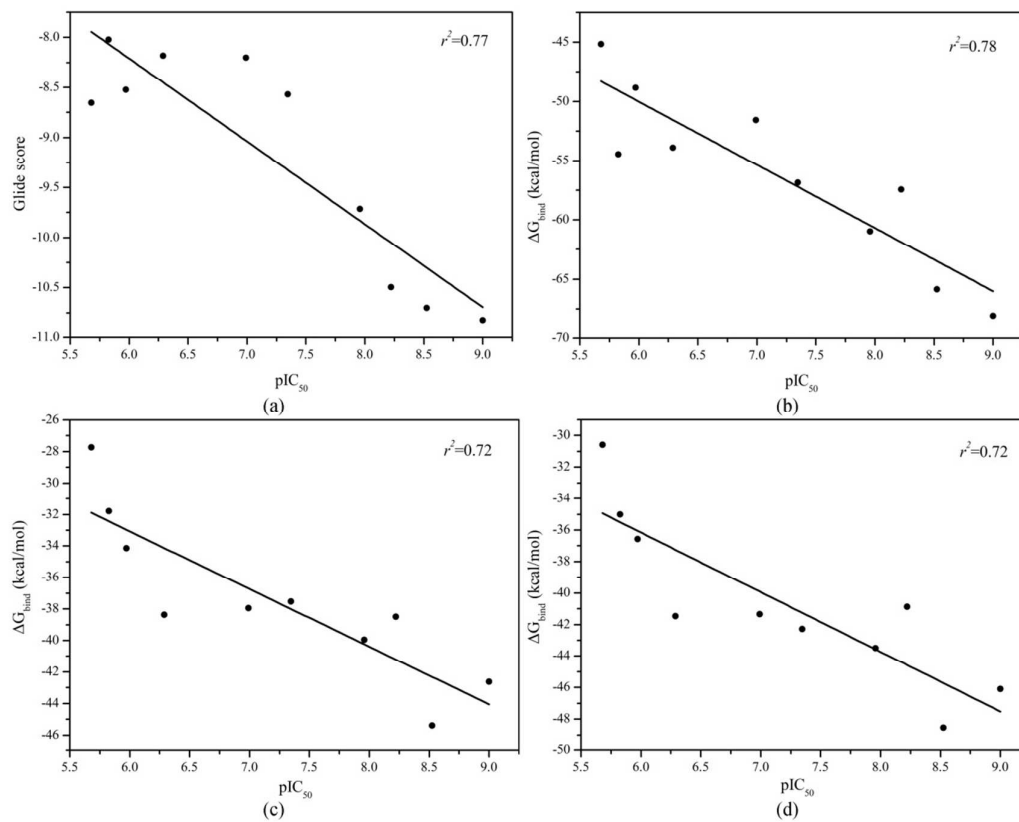


Figure 5

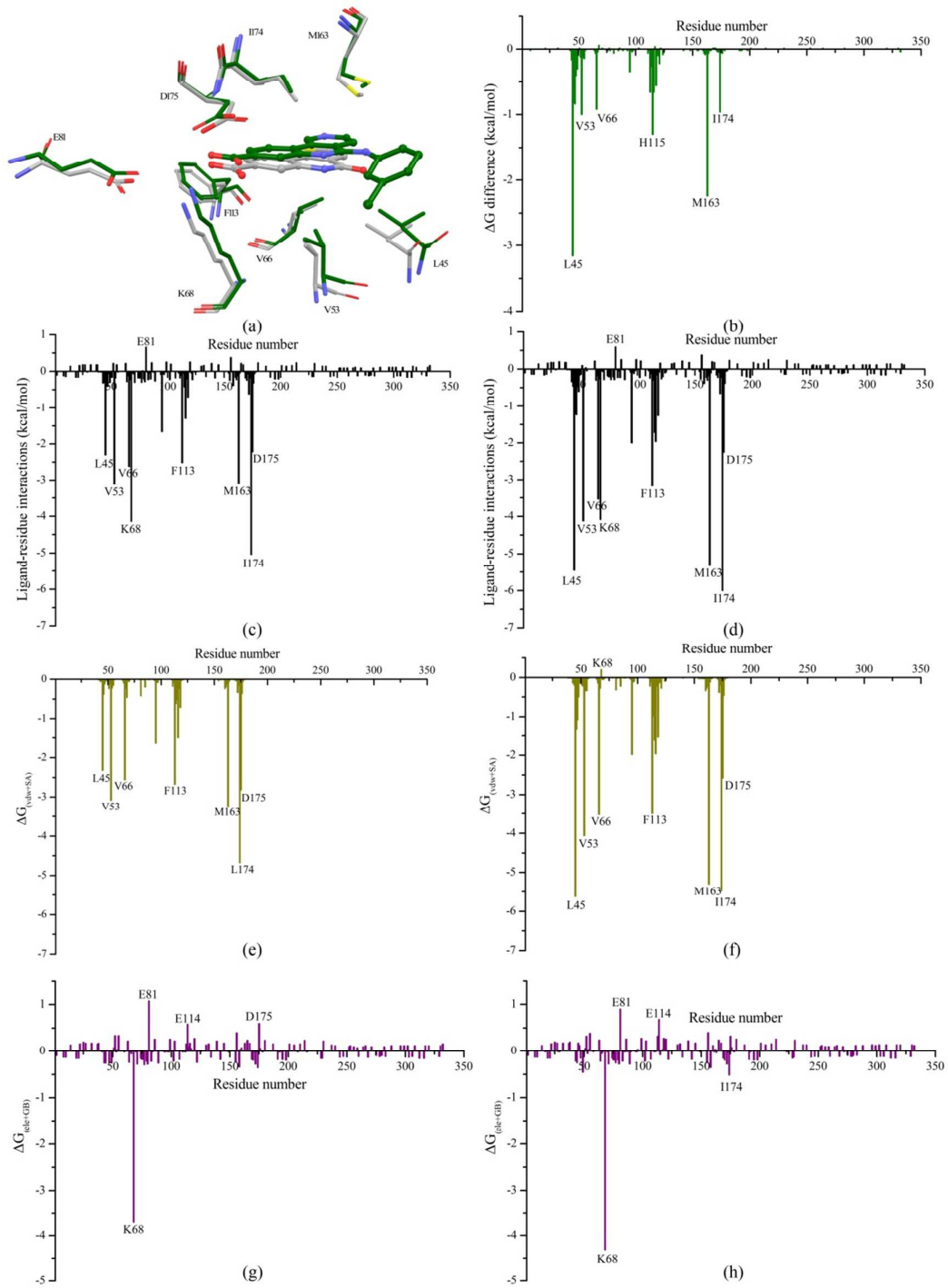


Figure 6

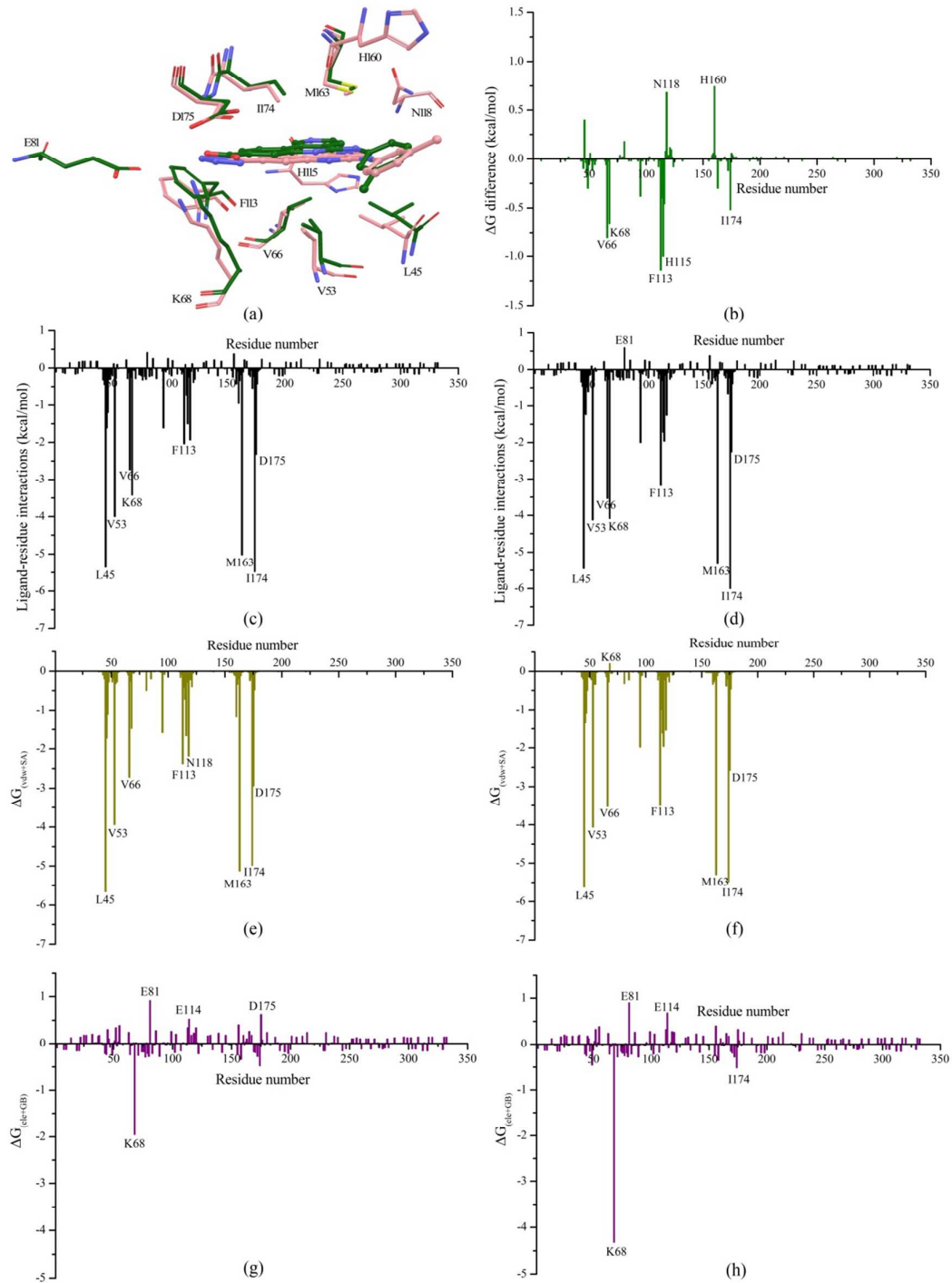


Figure 7

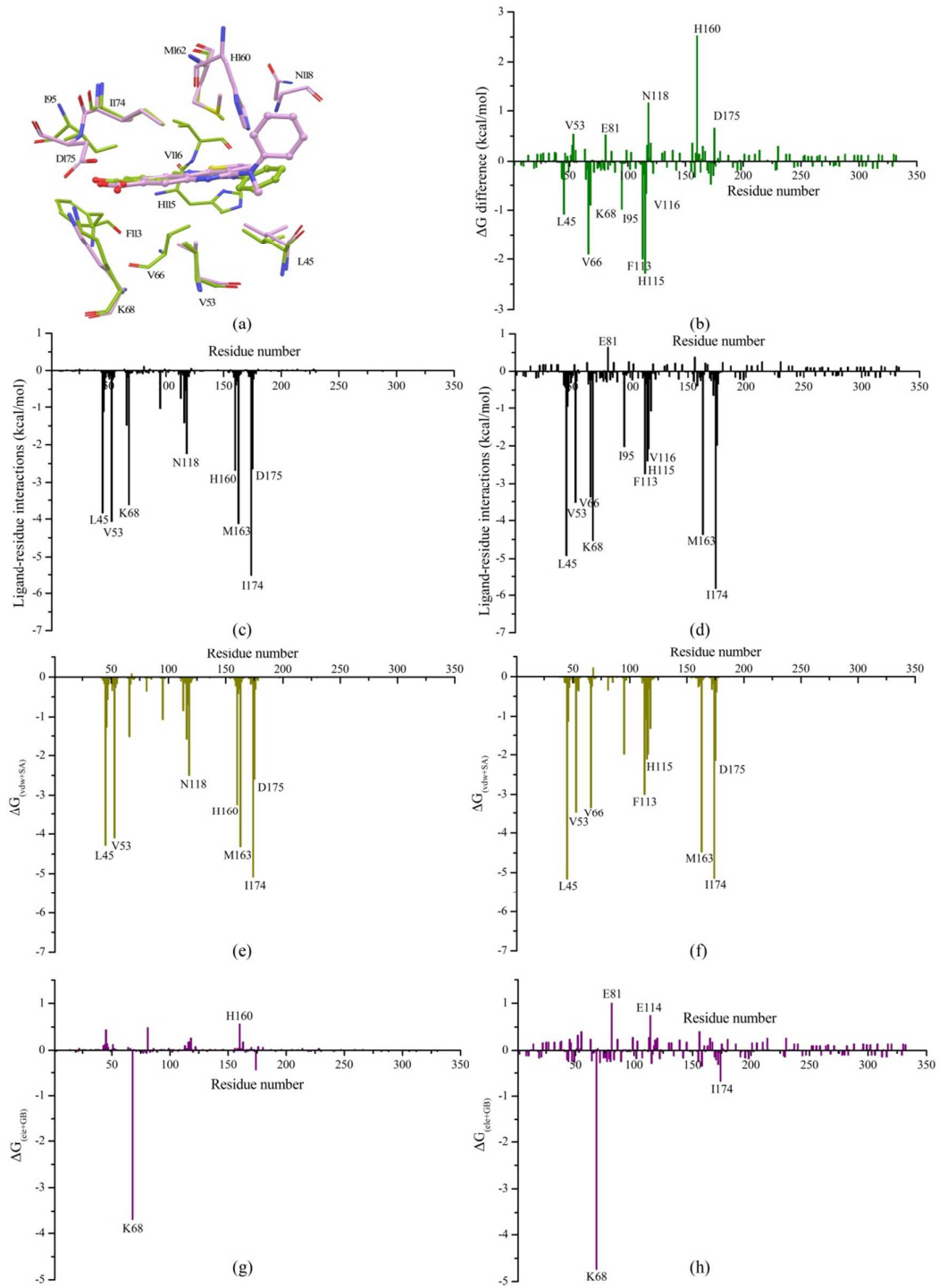


Figure 8